Dalton Transactions

ROYAL SOCIETY OF CHEMISTRY

PAPER

View Article Online
View Journal | View Issue

Cite this: *Dalton Trans.*, 2026, **55**, 3542

Flexible steric bulk of sugar wingtip substituents on bis(N-heterocyclic carbene) ligands of diplatinum complexes *via* chair–twist-boat conformational changes

Shuhei Nomura,[a] Itsuki Kobayashi,[a] Matsumi Doe,[b] Rika Tanaka,[b] Tamaki Nagasawa[b] and Takanori Nishioka *[a]

Received 16th January 2026,
Accepted 29th January 2026

DOI: 10.1039/d6dt00111d

rsc.li/dalton

In the *p*-toluenethiolate-bridged diplatinum complex bearing ethylene-bridged bis(N-heterocyclic carbene) ligands, all four acetyl-protected glucopyranosyl wingtip substituents adopt the chair conformation, giving rise to an open structure around the Pt_2S_2 core that allows the complex to react with a Grignard reagent. In contrast, in the corresponding diplatinum complex with *o*-xylene-bridged bis(N-heterocyclic carbene) ligands, two of the four acetyl-protected glucopyranosyl groups adopt the twist-boat conformation to relieve the steric repulsion among the wingtip *N*-substituents, resulting in a covered structure around the Pt_2S_2 core that inhibits reaction with a Grignard reagent.

Introduction

N-Heterocyclic carbenes (NHCs) are widely used ligands for transition metal complexes, which exhibit intriguing properties such as catalysis for olefin metathesis,[1] coupling reactions[2] and reduction of proton or CO_2.[3] Steric and electronic features of NHC ligands in complexes can be tuned by variation of wingtip *N*-substituents,[4] and the catalytic ability[5] and luminescence[6] behaviour of complexes bearing diverse *N*-substituents have been extensively investigated. BisNHC ligands, which consist of two NHC units with a bridging moiety such as methylene, 1,2-ethylene and 1,3-propylene, are particularly attractive because they stabilise transition metal complexes through the chelate effect. Moreover, the relative orientation of the two NHC units in such a bisNHC ligand with respect to the coordination plane of the metal centre in complexes depends on the lengths of the bridging moieties leading to variations of the dihedral angles between the NHC planes and the coordination plane[7] (Fig. 1). These geometric differences influence π-back-donation from the metal centre to the carbene carbon atoms as well as the steric repulsion between the wingtip *N*-substituents, thereby affecting the redox potentials and the catalytic abilities of their complexes, respectively.[8]

In our previous reports, glucopyranosyl groups were introduced into NHC ligands to develop water-soluble complex catalysts for coupling reactions in aqueous media.[9] The incorporated D-glucopyranosyl groups not only enhanced the water-solubility of complexes but also functioned as bulky substituents. Moreover, glucopyranosyl units can adopt the chair or twist-boat conformation depending on the steric demands of their local environments. For example, a monodentate NHC ligand bearing acetyl-protected α-D-glucopyranosyl and 2-pycolyl groups as the *N*-substituents affords the chiral-at-metal rhodium and iridium Cp* complexes with the

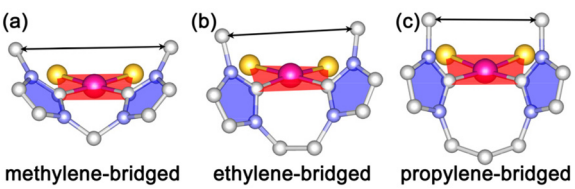

	NHC - M	$C_{Me}\cdots C_{Me}$
methylene-bridged	39.5(4)–46.5(3) [42(2)]	6.02(2)–6.45(2) [6.20(15)]
ethylene-bridged	55.4(4)–64.0(3) [59(4)]	5.06(1)–5.30(2) [5.23(6)]
propylene-bridged	70.9(2)	4.326(9)

Fig. 1 Ligand geometries of (a) methylene-, (b) ethylene- and (c) propylene-bridged bisNHC ligands in triplatinum complexes and table of dihedral angles (°, range [average]) between each NHC plane (blue) and coordination plane (red) (NHC–M) and distances (Å, range [average]) between wingtip *N*-methyl carbon atoms in each bisNHC ligand ($C_{Me}\cdots C_{Me}$, double-headed arrows) obtained from crystallographic analyses of triplatinum complexes.[8k,l]

[a]*Department of Chemistry, Graduate School of Science, Osaka Metropolitan University, Osaka 558-8585, Japan. E-mail: nishioka@omu.ac.jp*
[b]*Analytical Research Centre, Osaka Metropolitan University, Osaka 558-8585, Japan*

S-configuration, whereas the complexes bearing the corresponding β-D-glucopyranosyl ligand gave the *R*-configuration of the complexes. The α-D-glucopyranosyl units in the complexes adopt the twist-boat conformation due to steric repulsion and act like the L-glucopyranosyl groups.[10]

Inspired by these findings, we sought to control the steric environments around the metal centres by using the acetyl-protected β-D-glucopyranosyl (AcGlc) groups as wingtip *N*-substituents of bisNHC ligands bearing either a 1,2-ethylene (bisNHC-C2) or an *o*-xylene bridge (bisNHC-C4), which are expected to affect the spatial disposition of the wingtip *N*-substituents. This concept was applied to C–S coupling reactions, in which bulky ligands are proposed to promote reductive elimination of the C–S coupling product despite the strong affinity of sulfur atoms to transition metal ions.[11] Herein, we report the syntheses and structural characterisation of bis(*p*-toluenethiolate)-bridged diplatinum complexes bearing bisNHC-C2 or -C4 ligands (Scheme 1). In the bisNHC-C4 complex, two of the four AcGlc groups adopt the twist-boat conformation, resulting in a covered structure around the Pt_2S_2 core. Whereas the bisNHC-C2 complex, which features an open cavity composed of AcGlc units, reacts with 2-fluorophenylmagnesium bromide, the covered structure of the bisNHC-C4 complex suppresses the corresponding reaction.

Results and discussion

Structures of diplatinum complexes

The diplatinum complexes bearing the ethylene-bridged bisNHC-C2, $[\{Pt(bisNHC\text{-}C2)\}_2\{\mu\text{-}(S\text{-}p\text{-}tol)\}_2](PF_6)_2$ ($[\mathbf{1}](PF_6)_2$, Fig. 2), and the *o*-xylene-bridged bisNHC-C4, $[\{Pt(bisNHC\text{-}C4)\}_2\{\mu\text{-}(S\text{-}p\text{-}tol)\}_2](PF_6)_2$ ($[\mathbf{2}](PF_6)_2$, Fig. 3), were analysed by X-ray crystallography. Both complexes feature a Pt_2S_2 core supported by two bridging *p*-toluenethiolate ligands and two chelating bisNHC ligands. The dicationic moiety $[\mathbf{1}]^{2+}$ possesses a crystallographic two-fold axis passing through the centre of the Pt_2S_2 core, whereas $[\mathbf{2}]^{2+}$ exhibits a non-crystallographic two-fold axis. The Pt–S distances (2.362(2) and 2.370(2) Å for $[\mathbf{1}]^{2+}$, 2.310(3)–2.330 Å for $[\mathbf{2}]^{2+}$), S–Pt–S (84.12(7)° for $[\mathbf{1}]^{2+}$, 79.41(8)° and 79.68(8)° for $[\mathbf{2}]^{2+}$) and Pt–S–Pt (92.25(7)° for $[\mathbf{1}]^{2+}$, 91.01(8)° and 91.22(8)° for $[\mathbf{2}]^{2+}$) angles are all within the ranges reported for diplatinum complexes bridged by benzenethiolate or related ligands (Pt–S, 2.285(1)–2.440(3) Å; S–Pt–S, 80.03(4)°–85.3(1)°; Pt–S–Pt, 84.55(8)°–99.97(4)°), within experimental error. Notably, however, the *p*-toluenethiolate ligands in both $[\mathbf{1}]^{2+}$ and $[\mathbf{2}]^{2+}$ adopt a *syn*-arrangement, whereas previously reported complexes exclusively exhibit *anti*-arrangements.[12] The preference for the *syn*-arrangements of $[\mathbf{1}]^{2+}$ and $[\mathbf{2}]^{2+}$ is most likely a consequence of the substantial steric demand imposed by the AcGlc substituents.

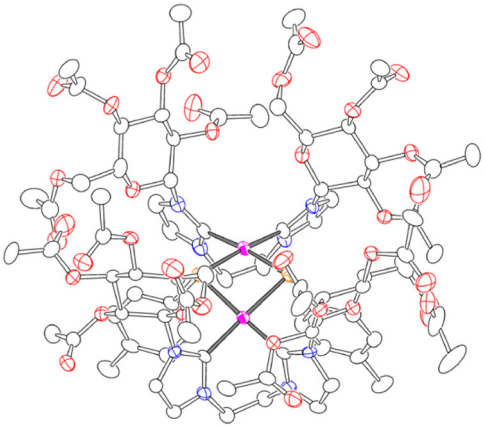

Fig. 2 Structure of the cationic moiety of the *p*-toluenethiolate-bridged diplatinum complex bearing ethylene-bridged bisNHC-C2 ligands, $[\mathbf{1}]^{2+}$. Disordered AcGlc units and hydrogen atoms are omitted for clarity (Pt, magenta; S, orange; O, red; N, blue; C, black). Selected interatomic distances (Å) and angles (°): Pt···Pt 3.4109(6); Pt–S 2.362(2), 2.370(2); S–Pt–S 84.12(7), Pt–S–Pt 92.25(7).

The most remarkable structural difference between the complexes lies in the conformation of the acetyl-protected β-D-glucopyranosyl (AcGlc) substituents. In the bisNHC-C2 complex $[\mathbf{1}]^{2+}$, all the AcGlc units adopt the chair conformation, whereas each bisNHC-C4 ligand in $[\mathbf{2}]^{2+}$ bears one chair and one twist-boat AcGlc moiety. This conformational divergence arises from steric repulsion between the AcGlc substituents. The distances between the anomeric carbon atoms of the glucopyranosyl groups within each bisNHC ligand are 5.34(1) Å for $[\mathbf{1}]^{2+}$ and 3.96(2) and 4.05(2) Å for $[\mathbf{2}]^{2+}$, indicating significantly closer proximity of the AcGlc units in $[\mathbf{2}]^{2+}$. These differences originate from the relative orientations of the NHC planes imposed by the bridging moieties. The *o*-xylene bridge, which is longer yet sterically constrained, enforces larger dihedral angles between the coordination plane and the NHC

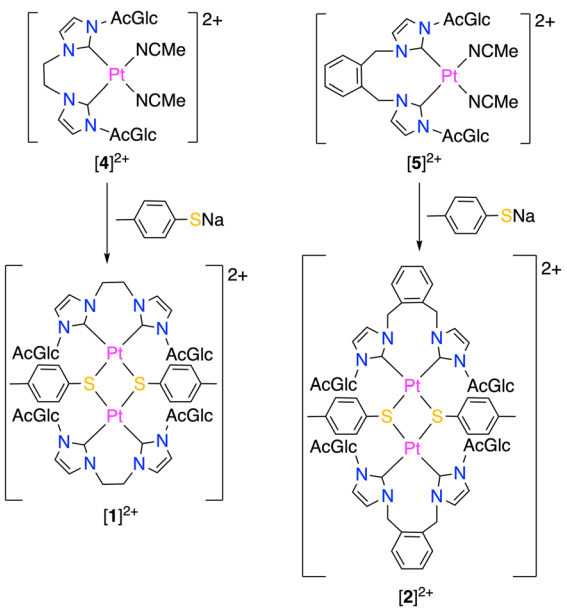

Scheme 1 Syntheses of Pt complexes bearing ethylene-bridged bisNHC-C2 and *o*-xylene-bridged bisNHC-C4 ligands with acetyl-protected glucopyranosyl wingtip substituents.

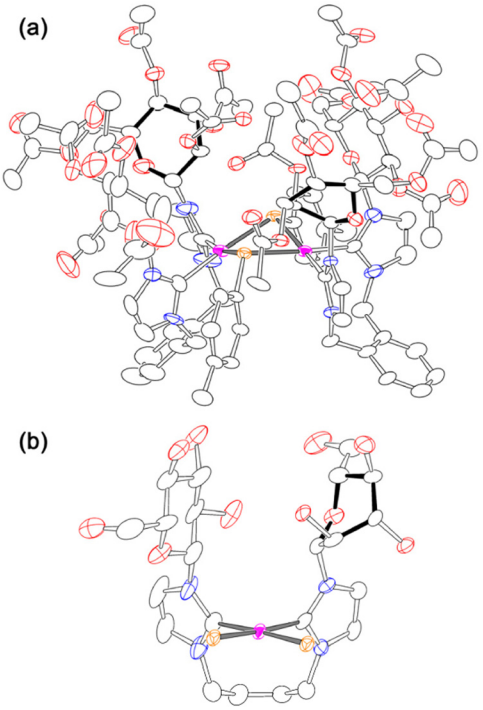

Fig. 3 (a) Structure of the cationic moiety of the *p*-toluenethiolate-bridged diplatinum complex bearing *o*-xylene-bridged bisNHC-C4 ligands, $[\mathbf{2}]^{2+}$. Disordered AcGlc units and hydrogen atoms are omitted for clarity (Pt, magenta; S, orange; O, red; N, blue; C, black). Selected interatomic distances (Å) and angles (°): Pt···Pt 3.3103(9); Pt–S 2.310(3), 2.313(3), 2.320(3), 2.330(3); S–Pt–S 79.41(8), 79.68(8); Pt–S–Pt 91.01(8), 91.22(8). (b) One of the {Pt(bisNHC-C4)} units bearing chair and twist-boat AcGlc wingtip substituents. Chair and twist-boat AcGlc groups are indicated with white open and black filled bonds, respectively. The acetyl groups and part of the xylene ring are omitted for clarity.

planes (72.7° and 73.0° for NHCs bearing chair-form AcGlc substituents and 80.6° and 80.8° for those bearing twist-boat AcGlc substituents), thereby enhancing steric repulsion between the AcGlc moieties. Consequently, one of the two AcGlc substituents in each bisNHC-C4 ligand adopts a twist-boat conformation. In contrast, the dihedral angles in $[\mathbf{1}]^{2+}$ (54.3° and 67.5°) are sufficiently small to allow all four AcGlc substituents to retain the chair conformation. The influence of steric repulsion is also reflected in the dihedral angles between the coordination planes of the two Pt centres, which is smaller in $[\mathbf{2}]^{2+}$ (139.3°) than in $[\mathbf{1}]^{2+}$ (146.6°), thereby reducing steric repulsion between the AcGlc substituents. In addition, the AcGlc units with the chair conformation in $[\mathbf{1}]^{2+}$ form a cavity above the Pt_2S_2 core (Fig. 4(a)), which is occupied by one of the two crystallographically independent PF_6^- counter anions in the solid state. In contrast, the Pt_2S_2 unit in $[\mathbf{2}]^{2+}$ is completely shielded by the AcGlc substituents (Fig. 4(b)). Although excessively bulky substituents on ligands often prevent complex formation with transition metal ions, the AcGlc groups here adapt their conformation from chair to twist-boat, providing an appropriate steric environment around the metal centres and thereby enabling complex formation. Other sterically adaptable NHC ligands have been reported for monodentate[13] and bidentate dinucleating systems,[14] and such adaptations typically rely on flexible hydrocarbon frameworks. In contrast, our system achieves steric modulation through conformational changes of sugar-based wingtip substituents.

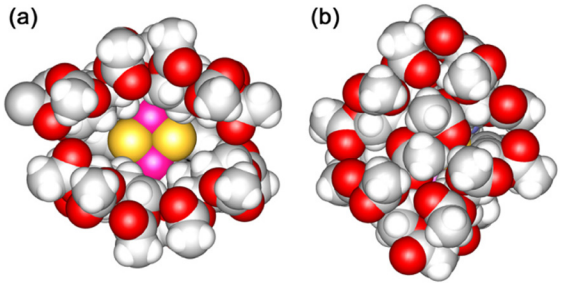

Fig. 4 Space-filling models of *p*-toluenethiolate-bridged diplatinum complexes (Pt, magenta; S, yellow; O, red; N, blue; C, grey; H, white) with (a) ethylene-bridged bisNHC-C2 ligands $[\mathbf{1}]^{2+}$ (**4c** isomer) and (b) *o*-xylene-bridged bisNHC-C4 ligands $[\mathbf{2}]^{2+}$ (**2c–2tb** isomer) obtained by crystallographic analyses.

The structures of $[\mathbf{1}]^{2+}$ and $[\mathbf{2}]^{2+}$ in the solid state are preserved in solution, as confirmed by ^{1}H NMR measurements. The signals of the 1-Glc protons in $[\mathbf{1}]^{2+}$ appeared as two doublets ($^3J_{H-H}$ = 9.3, 10.5 Hz, Fig. S7 in the SI), whereas in $[\mathbf{2}]^{2+}$ they were observed as a doublet ($^3J_{H-H}$ = 9.5 Hz) and a singlet (Fig. 5). This distinct signal pattern for $[\mathbf{2}]^{2+}$ clearly indicates that two of the four AcGlc units retain the twist-boat conformation even in solution. Consistent with this assignment, the $H_{1\text{-Glc}}$–C–C–$H_{2\text{-Glc}}$ torsion angles in the twist-boat AcGlc units of $[\mathbf{2}]^{2+}$ are 91° and 94°, as determined by the X-ray structural analysis, accounting for the absence of coupling between $H_{1\text{-Glc}}$ and $H_{2\text{-Glc}}$ according to the Karplus relationship. Other signals associated with the twist-boat glucopyranosyl frameworks also exhibited smaller coupling constants with the neighbouring protons, reflecting the near-orthogonal H–C–C–H torsion angles. In addition, ^{19}F and ^{31}P NMR spectra of the bisNHC-C2 complex $[\mathbf{1}](PF_6)_2$ showed only one doublet and one septet signal for the PF_6^- anion, respectively (Fig. S9 and S10 in the SI). These observations indicate that the PF_6^-

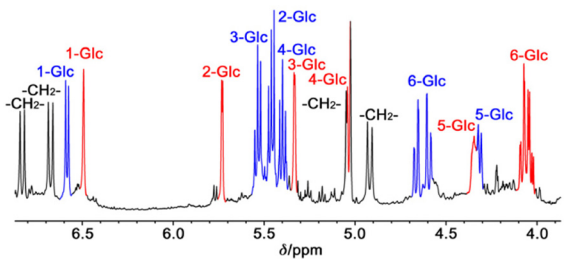

Fig. 5 ^{1}H NMR spectrum of the diplatinum complex bearing bisNHC-C4 ligands, $[\mathbf{2}](PF_6)_2$, in the region corresponding to the glucopyranosyl framework. Signals arising from glucopyranosyl units in the chair and twist-boat conformations are coloured blue and red, respectively.

anions, which occupy the cavity formed by the AcGlc units of $[\mathbf{1}]^{2+}$ in the solid state, either are released from the cavity or undergo rapid exchange with free PF_6^- anions in solution on the NMR timescale.

DFT calculations of possible isomers of diplatinum complexes

Density functional theory (DFT) calculations were performed on selected isomers of $[\mathbf{1}]^{2+}$ and $[\mathbf{2}]^{2+}$ to evaluate steric effects arising from the AcGlc substituents. The isomers considered include those bearing four chair AcGlc units (**4c**), two chair and two twist-boat units arranged as observed in the crystallography for $[\mathbf{2}]^{2+}$ (**2c–2tb**), the corresponding isomer in which the chair and twist-boat positions in the **2c–2tb** isomer are interchanged (**2tb–2c**) and an isomer containing four twist-boat units (**4tb**).

The optimised structure of $[\mathbf{1}]^{2+}$ (**4c** isomer, Fig. 6(a)) closely reproduces the X-ray crystal structure, showing an open cavity formed by the AcGlc substituents of the bisNHC ligands. Calculations for the $[\mathbf{1}]^{2+}$ series show that the **4c** isomer is the most stable among those examined (Table 1), which is consistent with the crystallographic data and solution NMR measurements. In contrast, the optimised structures of the **2c–2tb** (Fig. 6(b)), **2tb–2c** and **4tb** (Fig. S23 in the SI) isomers exhibit covered arrangement of the AcGlc groups. The **2tb–2c** isomer is thermodynamically less stable than the **2c–2tb** isomer (ΔG = +43.1 kJ mol^{-1}), reflecting the more congested disposition of the D-glucopyranosyl units. In comparison, the **4tb** isomer provides greater spatial separation among the AcGlc substituents and therefore is more stable than the **2tb–2c** isomer. These results indicate that both the combination and relative arrangement of chair and twist-boat conformations of the AcGlc units are key factors governing the stability of the isomers.

The optimised structure of $[\mathbf{2}]^{2+}$ (**2c–2tb** isomer, Fig. 6(d)) reproduces the covered arrangement of the AcGlc substituents observed in the solid state. In contrast, the **4c** isomer (Fig. 6(c)) adopts an open-cavity structure similar to that of the bisNHC-C2 complex $[\mathbf{1}]^{2+}$. DFT calculations indicate that the **2c–2tb** isomer is less stable than the **4c** isomer, which is inconsistent with the observations in the solid state and in solution. However, the free-energy difference between the **4c** and **2c–2tb** isomers of $[\mathbf{2}]^{2+}$ (ΔG = +7.1 kJ mol^{-1}) is substantially smaller than that of $[\mathbf{1}]^{2+}$ (ΔG = +44.5 kJ mol^{-1}). This small energy difference suggests that the covered structure of the **2c–2tb** isomer of $[\mathbf{2}]^{2+}$ is stabilised by additional factors, such as crystal packing in the solid state and solvation in solution. In addition, as observed for the bisNHC-C2 complex $[\mathbf{1}]^{2+}$, the **4tb** isomer of $[\mathbf{2}]^{2+}$ is more stable than the **2tb–2c** isomer.

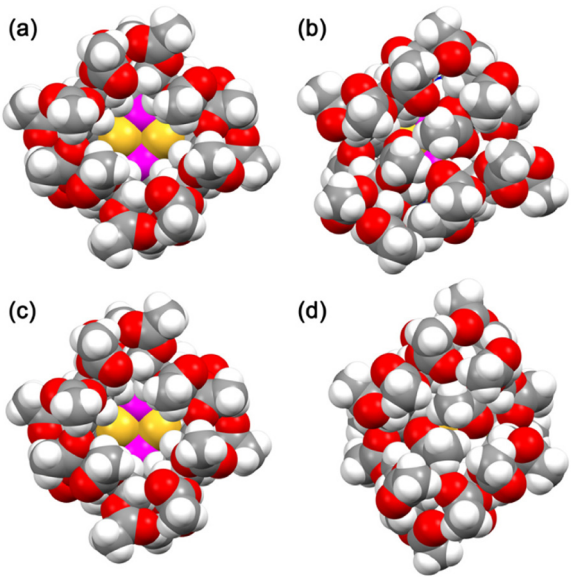

Fig. 6 Optimised structures of the (a) **4c** isomer of $[\mathbf{1}]^{2+}$, (b) **2c–2tb** isomer of $[\mathbf{1}]^{2+}$, (c) **4c** isomer of $[\mathbf{2}]^{2+}$ and (d) **2c–2tb** isomer of $[\mathbf{2}]^{2+}$ (Pt, magenta; S, yellow; O, red; N, blue; C, grey; H, white).

Table 1 Differences in Gibbs free energies (kJ mol^{-1}) between **4c** and the other isomers of diplatinum complexes $[\mathbf{1}]^{2+}$ and $[\mathbf{2}]^{2+}$ obtained by DFT calculations[a]

	4c	2c–2tb	2tb–2c	4tb
$[\mathbf{1}]^{2+}$	0	44.5	87.6	54.3
$[\mathbf{2}]^{2+}$	0	7.1	99.8	58.0

[a] Details of the data are listed in Tables S11 and S12 in the SI.

Reactions of diplatinum complexes with Grignard reagents

The reactions of $[\mathbf{1}]^{2+}$ and $[\mathbf{2}]^{2+}$ with 2-fluorophenylmagnesium bromide were investigated by ^{19}F NMR spectroscopy and electrospray ionisation mass spectrometry (Scheme 2).

Upon treatment of the bisNHC-C2 complex, $[\mathbf{1}](PF_6)_2$, with 2-fluorophenyl-magnesium bromide in the presence of CuI in THF under a N_2 atmosphere, the ^{19}F NMR spectrum of the product showed a singlet signal at approximately −141 ppm

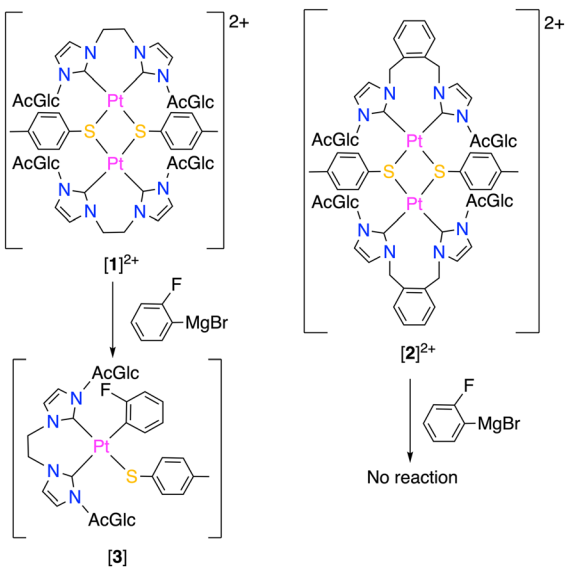

Scheme 2 Reaction of Pt complexes bearing ethylene-bridged bisNHC-C2 $[\mathbf{1}]^{2+}$ and *o*-xylene-bridged bisNHC-C4 ligands $[\mathbf{2}]^{2+}$ with 2-fluorophenylmagnesium bromide.

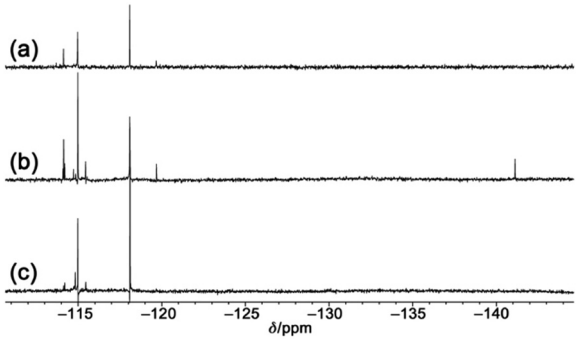

Fig. 7 ^{19}F NMR spectra of (a) decomposition products of 2-fluorophenylmagnesium bromide (2-FPhMgBr), (b) products of the reaction of the bisNHC-C2 complex [**1**](PF$_6$)$_2$ with 2-FPhMgBr and (c) products of the reaction of the bisNHC-C4 complex [**2**](PF$_6$)$_2$ with 2-FPhMgBr.

(Fig. 7(b)), in addition to several signals attributable to decomposition products of the Grignard reagent (Fig. 7(a)). This upfield-shifted signal is consistent with the formation of a mononuclear platinum complex, [Pt(bisNHC-C2)(Ph-2-F)(S-*p*-tol)] ([**3**]). The mass spectrum of the product exhibited signals at $m/z \approx 1234$ and 1112, assignable to [**3**–H]$^+$ and [**3**–(S-*p*-tol)]$^+$, respectively (Fig. S19 in the SI), supporting the formation of [**3**]. In contrast, the product of the corresponding reaction of the *o*-xylene-bridged complex [**2**](PF$_6$)$_2$ did not show any ^{19}F NMR signal attributable to a 2-fluorophenyl-coordinated platinum species (Fig. 7(c)). This remarkable difference in reactivity can be attributed to the distinct steric environments in [**1**]$^{2+}$ and [**2**]$^{2+}$. The open cavity of [**1**]$^{2+}$, defined by four chair AcGlc substituents, allows access of the Grignard reagent to the platinum centres, whereas the covered structure of [**2**]$^{2+}$, formed by two chair and two twist-boat AcGlc units, sterically blocks approach to the metal centres.

The thermal decomposition of [**3**] was examined to probe the formation of the C–S coupling product, (2-fluorophenyl)(4-tolyl)sulfide (Scheme 3). A crude sample containing [**3**], obtained from the reaction of [**1**](PF$_6$)$_2$ with 2-fluorophenylmagnesium bromide in acetonitrile, was heated at 80 °C for 17 h. The ^{19}F NMR spectrum of the residue obtained after removal of the solvent displayed a small singlet signal at −109.8 ppm (Fig. S22 in the SI), which is consistent with the reported chemical shift for the ^{19}F NMR signal of (2-fluorophenyl)(4-tolyl)sulfide (−110.1 to −109.9 ppm).[15]

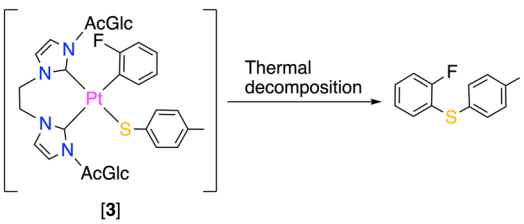

[**3**]

Scheme 3 Thermal decomposition reaction of Pt complex [**3**] generated by the reaction of ethylene-bridged bisNHC-C2 [**1**]$^{2+}$ with 2-fluorophenylmagnesium bromide.

Conclusions

We synthesised *p*-toluenethiolate-bridged diplatinum complexes supported by bisNHC ligands bearing acetyl-protected glucopyranosyl (AcGlc) groups as wingtip *N*-substituents and either an ethylene or an *o*-xylene linker between two NHC units. The steric repulsion among the AcGlc substituents strongly depends on the length of the bridging moiety and is more pronounced in the *o*-xylene-bridged complex, which features a longer and yet sterically restricted bridging unit. This congestion includes a conformational change of two of the four glucopyranosyl units from chair to twist-boat, thereby relieving steric repulsion. As a consequence, the *o*-xylene-bridged complex adopts a covered structure, in which the AcGlc substituents shield the metal centres, preventing reaction with a Grignard reagent. In contrast, the ethylene-bridged complex forms an open cavity defined by the AcGlc units around the metal centres, allowing access of the Grignard reagent to the platinum centres and leading to the formation of a mononuclear platinum complex bearing *p*-tolylthiolate and 2-fluorophenyl ligands. Subsequent thermal decomposition of this complex affords (2-fluorophenyl)(4-tolyl)sulfide as the C–S coupling product.

Our results demonstrate that the bridging moieties of bisNHC ligands provide an effective means to tune the steric repulsion between wingtip substituents. Although excessively bulky ligand substituents often impede complex formation, precise control of steric demand enables the generation of an optimal steric environment. In this context, the AcGlc groups adapt their conformation from chair to twist-boat, thereby relieving steric congestion while maintaining sufficient steric protection around the metal centres to allow complex formation. These finding highlight the utility of sugar units as bulky substituents that can automatically modulate steric repulsion through conformational flexibility without inhibiting coordination to metal ions. Given the wide diversity of accessible three-dimensional structures of pyranoses, such motifs represent promising candidates for the design of sterically adaptive ligands capable of fine-tuning the coordination environments of metal complexes.

Experimental

General procedures

All chemicals were purchased from Sigma-Aldrich, Nacalai Tesque and Wako Pure Chemical Industries and were used as received without further purification. [(bisNHC-C2)H$_2$](PF$_6$)$_2$ was prepared according to a reported procedure.[9d] ^{1}H, ^{13}C and ^{19}F NMR spectra were recorded on a Bruker AVANCE 400 or 600 FT-NMR spectrometer. Chemical shifts (δ, ppm) and coupling constants (J, Hz) for ^{1}H and ^{13}C NMR signals are reported relative to SiMe$_4$ and were referenced to residual solvent resonances. Chemical shifts for ^{19}F signals were externally referenced to CFCl$_3$. Elemental analyses were performed on a J-Science Lab JM-10 elemental analyser. Electrospray ionisation

mass spectrometry was performed on a JEOL AccuTOF LC-plus JMS-T100LP spectrometer.

Synthesis of the bisNHC ligand precursor bearing an *o*-xylene bridge and acetyl-protected β-D-glucopyranosyl groups ([(bisNHC-C4)H_2] (PF_6)$_2$)

A mixture of α,α′-dibromo-*o*-xylene (0.48 g, 1.6 mmol) and 1-(2,3,4,6-tetra-*O*-acethyl-β-D-glucopyranosyl)imidazole (2.1 g, 5.3 mmol) in MeCN (25 mL) was heated at 70 °C for 24 h in a sealed tube. The solvent was removed under reduced pressure to afford a white solid, which was treated with water. Insoluble solids were removed by filtration and NH_4PF_6 (1.4 g, 8.5 mmol) was added to the filtrate to give the corresponding hexafluorophosphate salt as a white precipitate. The product was collected by filtration and air-dried. Yield: 1.6 g (85%). MS (ESI+, CH_3CN): *m*/*z* = 569.27 (569.23 calcd for [(bisNHC-C4)H_2–AcGlc]$^+$), 1045.29 (1045.41 calcd for [(bisNHC-C4)H_2 + PF_6]$^+$). ^{1}H NMR (DMSO-d_6, 400 MHz, 298 K): δ 9.62 (2-Im, s, 2H), 8.17 (5-Im, s, 2H), 7.85 (4-Im, s, 2H), 7.50 (4-, 5-Xy, dd, 2H, J = 5.7 Hz, 3.4 Hz), 7.22 (3-, 6-Xy, dd, 2H, J = 5.6 Hz, 3.5 Hz), 6.04 (1-Glc, d, 2H, ^3J = 8.3 Hz), 5.66–5.51 (CH_2, 3-Glc, 2-Glc, m, 8H), 5.27 (4-Glc, t, 2H, ^3J = 9.6 Hz), 4.39 (5-Glc, dt, 2H, ^3J = 10.0, 4.0 Hz), 4.16 (6-Glc, d, 2H, ^3J = 3.7 Hz), 2.04 (Me_{AcO}, s, 3H), 2.01 (Me_{AcO}, s, 3H), 1.98 (Me_{AcO}, s, 3H), 1.90 (Me_{AcO}, s, 3H). ^{13}C NMR (DMSO-d_6, 100 MHz, 298 K): δ 170.1 (CO_{AcO}), 169.6 (CO_{AcO}), 169.5 (CO_{AcO}), 169.2 (CO_{AcO}), 136.9 (Xy), 132.5 (Xy), 129.8 (2-Im), 129.3 (Xy), 123.7 (4-Im), 121.3 (5-Im), 83.7 (1-Glc), 73.8 (5-Glc), 71.3 (2- or 3-Glc), 71.0 (2- or 3-Glc), 67.2 (4-Glc), 61.7 (6-Glc), 49.5 (CH_2), 20.6 (Me_{AcO}), 20.4 (Me_{AcO}), 20.2 (Me_{AcO}), 20.0 (Me_{AcO}).

Synthesis of [Pt(bisNHC-C2)(NCMe)$_2$](PF_6)$_2$ ([4](PF_6)$_2$)

A mixture of [(bisNHC-C2)H_2](PF_6)$_2$ (558 mg, 0.50 mmol), K_2[$PtCl_4$] (208 mg 0.50 mmol) and NaOAc (123 mg, 1.50 mmol) in DMSO (30 mL) was heated at 70 °C for 28 h in a sealed tube to give an orange solution. NH_4Cl (265 mg, 0.50 mmol) was added, and the mixture was stirred for 1 h. The solvent was removed under reduced pressure, and the resulting white solid was triturated with water, collected by filtration and air-dried. A suspension of the white solid and KI, which was ground in a mortar, in CH_2Cl_2 (40 mL) was stirred at room temperature for 48 h. The insoluble solid was removed by filtration, and the filtrate was washed with water (3 × 20 mL). The organic layer was separated and dried over $MgSO_4$, and the solvent was removed under reduced pressure to give a yellow solid. The solid was dissolved in MeCN (30 mL), and $AgPF_6$ (253 mg, 1.0 mmol) was added. After stirring for 1 h, the resulting yellow solid was removed by filtration. After the solvent was removed under reduced pressure, Et_2O was added to the residue to afford the product as a white solid, which was collected by filtration and air-dried. Yield: 584 mg (84%). MS (ESI+, CH_3CN): *m*/*z* = 508.66 (508.62 calcd for [Pt(bisNHC-C2)]$^{2+}$), *m*/*z* = 1243.41 (1244.26 calcd for [{Pt(bisNHC-C2)(NCMe)$_2$} + PF_6]$^+$). ^{1}H NMR (CD_3CN, 600 MHz, 298 K): δ 7.46 (4-Im$_a$, d, 1H, ^3J = 2.2 Hz), 7.42 (4-Im$_b$, d, 1H, ^3J = 2.2 Hz), 7.35 (5-Im$_b$, d, 1H, ^3J = 2.1 Hz), 7.17 (5-Im$_a$, d, 1H, ^3J = 2.1 Hz), 6.32 (1-Glc$_a$, d, 1H, ^3J = 9.3 Hz), 6.26 (1-Glc$_b$, d, 1H, ^3J = 9.3 Hz), 5.59 (2-Glc$_a$, t, 1H, ^3J = 9.6 Hz), 5.534 (3-Glc$_a$ or 3-Glc$_b$, t, 1H, ^3J = 9.7 Hz), 5.528 (3-Glc$_a$ or 3-Glc$_b$, t, 1H, ^3J = 9.7 Hz), 5.47–5.44 (CH_2-Im$_b$, m, 1H), 5.45 (2-Glc$_b$, t, 1H, ^3J = 9.5 Hz), 5.41 (4-Glc$_a$, t, 1H, ^3J = 9.8 Hz), 5.27 (4-Glc$_b$, t, 1H, ^3J = 9.7 Hz), 4.76 (CH_2-Im$_a$, dt, 1H, ^2J = 14.9 Hz, ^3J = 4.1 Hz), 4.63 (CH_2-Im$_b$, dt, 1H, ^2J = 15.3 Hz, ^3J = 4.5 Hz), 4.60–4.58 (5-Glc$_a$, m, 1H), 4.55 (CH_2-Im$_a$, dt, 1H, ^2J = 15.0 Hz, ^3J = 5.3 Hz), 4.35 (5-Glc$_b$, ddd, 1H, ^2J = 10.0 Hz, ^3J = 3.7 Hz, ^3J = 2.8 Hz), 4.27 (6-Glc$_b$, dd, 1H, ^2J = 12.8 Hz, ^3J = 4.0 Hz), 4.23 (6-Glc$_a$, dd, 1H, ^2J = 13.2 Hz, ^3J = 1.9 Hz), 4.17 (6-Glc$_b$, dd, 1H, ^2J = 12.7 Hz, ^3J = 2.6 Hz), 4.12 (6-Glc$_a$, dd, 1H, ^2J = 13.2 Hz, ^3J = 2.4 Hz), 2.04 (Me_{AcO}, s, 3H), 2.021 (Me_{AcO}, s, 3H), 2.019 (Me_{AcO}, s, 3H), 1.99 (Me_{AcO}, s, 3H), 1.97 (Me_{AcO}, s, 3H), 1.91 (Me_{AcO}, s, 3H), 1.89 (Me_{AcO}, s, 3H), 1.23 (Me_{AcO}, s, 3H). ^{13}C NMR (CD_3CN, 150 MHz, 298 K): δ 171.3 (CO_{AcO}), 171.23 (CO_{AcO}), 171.20 (CO_{AcO}), 170.69 (CO_{AcO}), 170.67 (CO_{AcO}), 170.4 (CO_{AcO}), 170.1 (CO_{AcO}), 169.9 (CO_{AcO}), 137.3 (2-Im$_b$), 134.1 (2-Im$_a$), 127.0 (5-Im$_a$), 125.5 (5-Im$_b$), 120.9 (4-Im$_a$, 4-Im$_b$), 86.4 (1-Glc$_a$), 86.1 (1-Glc$_b$), 75.2 (5-Glc$_a$), 75.0 (5-Glc$_b$), 73.3 (3-Glc$_a$), 72.6 (3-Glc$_b$), 70.8 (2-Glc$_a$), 70.4 (2-Glc$_b$), 68.9 (4-Glc$_b$), 67.7 (4-Glc$_a$), 62.6 (6-Glc$_b$), 61.4 (6-Glc$_a$), 49.8 (CH_2-Im$_a$), 47.3 (CH_2-Im$_b$), 21.0 (Me_{AcO}), 20.93 (Me_{AcO}), 20.90 (Me_{AcO}), 20.82 (Me_{AcO}), 20.76 (Me_{AcO}), 19.6 (Me_{AcO}), 20.82 (Me_{AcO}), 20.76 (Me_{AcO}), 19.6 (Me_{AcO}).

Synthesis of [Pt(bisNHC-C4)(NCMe)$_2$](PF_6)$_2$ ([5](PF_6)$_2$)

[Pt(bisNHC-C4)(NCMe)$_2$](PF_6)$_2$ was synthesised following the same procedure as that used for [Pt(bisNHC-C2)(NCMe)$_2$](PF_6)$_2$, except that [(bisNHC-C4)H_2](PF_6)$_2$ (596 mg, 0.50 mmol) was used in place of [(bisNHC-C2)H_2](PF_6)$_2$. Yield: 588 mg (80%). MS (ESI+, CH_3CN): *m*/*z* = 546.67 (546.66 calcd for [Pt(bisNHC-C4)]$^{2+}$), *m*/*z* = 1320.44 (1320.30 calcd for [{Pt(bisNHC-C4)(NCMe)$_2$} + PF_6]$^+$). ^{1}H NMR (CD_3CN, 600 MHz, 298 K): δ 7.78 (4-, 5-Xy, m, 2H), 7.53 (3-, 6-Xy, m, 2H), 7.49 (5-Im$_a$, d, 1H, ^3J = 2.3 Hz), 7.48 (5-Im$_b$, d, 1H, ^3J = 2.3 Hz), 7.45 (4-Im$_b$, d, 1H, ^3J = 2.3 Hz), 7.42 (4-Im$_a$, d, 1H, ^3J = 2.3 Hz), 6.54 (1-Glc$_a$, d, 1H, ^3J = 8.9 Hz), 6.40 (CH_2-Im$_a$, d, 1H, ^2J = 15.1 Hz), 6.38 (CH_2-Im$_b$, d, 1H, ^2J = 14.9 Hz), 6.18 (1-Glc$_b$, d, 1H, ^3J = 9.4 Hz), 5.68 (2-Glc$_b$, 3-Glc$_a$, m, 2H), 5.47 (4-Glc$_a$, t, 1H, ^3J = 9.7 Hz), 5.36 (2-Glc$_a$, dd, 1H, ^3J = 10.0 Hz, ^3J = 8.9 Hz), 5.29 (3-Glc$_b$, 4-Glc$_b$, m, 2H), 5.20 (CH_2-Im$_b$, d, 1H, ^2J = 14.9 Hz), 5.16 (CH_2-Im$_a$, d, 1H, ^2J = 15.0 Hz), 4.51 (5-Glc$_a$, 5-Glc$_b$, m, 2H), 4.27 (6-Glc$_b$, d, 1H, ^3J = 2.8 Hz), 4.26 (6-Glc$_b$, d, 1H, ^3J = 2.8 Hz), 4.22 (6-Glc$_a$, dd, 1H, ^2J = 13.1 Hz, ^3J = 2.0 Hz), 4.12 (6-Glc$_a$, dd, 1H, ^2J = 13.1 Hz, ^3J = 2.6 Hz), 2.08 (Me_{AcO}, s, 3H), 2.05 (Me_{AcO}, s, 3H), 2.04 (Me_{AcO}, s, 3H), 2.01 (Me_{AcO}, s, 3H), 1.99 (Me_{AcO}, s, 3H), 1.97 (Me_{AcO}, s, 3H), 1.89 (Me_{AcO}, s, 3H), 1.42 (Me_{AcO}, s, 3H). ^{13}C NMR (CD_3CN, 150 MHz, 298 K): δ 171.4 (CO_{AcO}), 171.2 (CO_{AcO}), 171.1 (CO_{AcO}), 170.6 (CO_{AcO}), 170.3 (CO_{AcO}), 170.0 (CO_{AcO}), 169.7 (CO_{AcO}), 137.1 (2-Im$_b$), 136.3 (2-Im$_a$), 135.4 (1- or 2-Xy), 134.6 (1- or 2-Xy), 133.0 (3- or 6-Xy), 132.6 (3- or 6-Xy), 131.5 (4- or 5-Xy), 131.4 (4- or 5-Xy), 125.4 (5-Im$_a$), 124.5 (5-Im$_b$), 122.4 (4-Im$_b$), 122.0 (4-Im$_a$), 86.8 (1-Glc$_b$), 85.8 (1-Glc$_a$), 75.2 (5-Glc$_a$), 74.8 (5-Glc$_b$), 73.4 (3-Glc$_b$), 72.4 (3-Glc$_a$), 72.3 (2-Glc$_a$), 68.7 (2-Glc$_b$ and 4-Glc$_b$), 68.0 (4-Glc$_a$), 61.8 (6-Glc$_a$), 61.7 (6-Glc$_b$), 53.0 (CH_2-Im$_a$), 52.8 (CH_2-Im$_b$), 20.97

(Me_{AcO}), 20.95 (Me_{AcO}), 20.91 (Me_{AcO}), 53.0 (CH_{2a}), 52.8 (CH_{2b}), 20.97 (Me_{AcO}), 20.95 (Me_{AcO}), 20.91 (Me_{AcO}), 20.85 (Me_{AcO}), 20.83 (Me_{AcO}), 20.81 (Me_{AcO}), 20.4 (Me_{AcO}).

Synthesis of [{Pt(bisNHC-C2)}$_2${μ-(S-*p*-tol)}$_2$](PF$_6$)$_2$ ([1](PF$_6$)$_2$)

A mixture of *p*-toluenethiol (82 mg, 0.66 mmol) and NaOMe (60 mg, 1.10 mmol) in degassed MeOH (24 mL) was stirred for 1 h. The mixture was added to a solution of [Pt(bisNHC-C2)(NCMe)$_2$](PF$_6$)$_2$ (306 mg, 0.22 mmol) in MeCN (25 mL) and stirred for 3 h. The solvent was removed under reduced pressure to give a yellow solid, which was redissolved in MeCN. Insoluble solids were removed by filtration, and the solvent was removed under reduced pressure to afford a yellow crude product. The crude product was dissolved in CH_2Cl_2, and insoluble solids were removed by filtration through Celite. Addition of Et_2O to the filtrate gave a yellow solid, which was collected by filtration and air-dried. Yield: 220 mg (78%). Single crystals suitable for X-ray crystallographic analysis were obtained by recrystallisation of crude crystals, which were prepared by slow diffusion of *m*-xylene into a mixture of [Pt(bisNHC-C2)(NCMe)$_2$](PF$_6$)$_2$ and *p*-toluenethiol in MeCN, in CH_2Cl_2 by slow diffusion of toluene and MeOH. Anal. calcd for [**1**](PF$_6$)$_2$·2CH_2Cl_2 ($C_{88}H_{110}Cl_4F_{12}N_8O_{36}P_2Pt_2S_2$): C, 38.55; H, 4.04; N, 4.09. Found: C, 38.44; H, 4.28; N, 4.32. MS (ESI+, CH_3CN): *m*/*z* = 1140.73 (1140.27 calcd for [**1**]$^{2+}$ and [(**1**)/2]$^+$), 2425.49 (2425.51 calcd for [(**1**) + PF$_6$]$^+$). ^{1}H NMR (CD_3CN, 600 MHz, 298 K): δ 7.69 (2-tol, d, 4H, ^3J = 8.0 Hz), 7.11 (4-Im$_a$, d, 2H, ^3J = 1.8 Hz), 7.08 (4-Im$_b$, d, 2H, ^3J = 1.9 Hz), 6.952 (3-tol, d, 4H, ^3J = 7.7 Hz), 6.946 (1-Glc$_b$, d, 2H, ^3J = 10.5 Hz), 6.93 (5-Im$_a$, d, 2H, ^3J = 1.9 Hz), 6.79 (5-Im$_b$, d, 2H, ^3J = 1.7 Hz), 6.42 (1-Glc$_a$, d, 2H, ^3J = 9.3 Hz), 5.81 (CH_2-Im$_a$, m, 2H), 5.69 (2-Glc$_b$, t, 2H, ^3J = 9.7 Hz), 5.62 (3-Glc$_a$, t, 2H, ^3J = 9.6 Hz), 5.45 (2-Glc$_a$, t, 2H, ^3J = 9.9 Hz), 5.43 (3-Glc$_b$, t, 2H, ^3J = 10.1 Hz), 5.42 (4-Glc$_a$, t, 2H, ^3J = 10.0 Hz), 5.26 (4-Glc$_b$, t, 2H, ^3J = 9.8 Hz), 4.86 (6-Glc$_a$, d, 2H, ^3J = 12.4 Hz), 4.68 (5-Glc$_b$, d, 2H, ^3J = 9.9 Hz), 4.62 (5-Glc$_a$, d, 2H, ^3J = 10.0 Hz), 4.43 (6-Glc$_a$, dd, 2H, ^2J = 12.9 Hz, ^3J = 1.6 Hz), 4.36–4.29 (6-Glc$_b$, CH_2-Im$_a$, CH_2-Im$_b$, m, 6H), 4.13 (CH_2-Im$_b$, m, 2H, ^2J = 14.0 Hz), 2.20 (Me$_{tol}$, s, 6H), 2.091 (Me_{AcO}, s, 12H), 2.087 (Me_{AcO}, s, 6H), 2.06 (Me_{AcO}, s, 6H), 1.99 (Me_{AcO}, s, 6H), 1.93 (Me_{AcO}, s, 6H), 1.63 (Me_{AcO}, s, 6H), 1.31 (Me_{AcO}, s, 6H). ^{13}C NMR (CD_3CN, 150 MHz, 298 K): δ 171.5 (CO_{AcO}), 171.4 (CO_{AcO}), 171.3 (CO_{AcO}), 170.9 (CO_{AcO}), 170.8 (CO_{AcO}), 170.7 (CO_{AcO}), 170.4 (CO_{AcO}), 170.2 (CO_{AcO}), 157.6 (2-Im$_a$), 153.0 (2-Im$_b$), 138.5 (1-tol), 133.4 (2-tol), 132.9 (4-tol), 130.2 (3-tol), 125.4 (5-Im$_b$), 123.1 (5-Im$_a$), 119.8 (4-Im$_a$), 119.7 (4-Im$_b$), 86.1 (1-Glc$_b$), 85.6 (1-Glc$_a$), 75.8 (5-Glc$_b$), 74.7 (5-Glc$_a$), 74.1 (3-Glc$_b$), 73.0 (3-Glc$_a$), 70.6 (2-Glc$_a$), 69.3 (4-Glc$_b$), 68.9 (2-Glc$_b$), 68.4 (4-Glc$_a$), 62.7 (6-Glc$_a$), 61.3 (6-Glc$_b$), 49.8 (CH_2-Im$_b$), 46.9 (CH_2-Im$_a$), 21.22 (Me_{AcO}), 21.15 (Me_{AcO}), 21.0 (Me_{AcO}), 20.93 (Me_{AcO}), 20.90 (Me$_{tol}$), 20.8 (Me_{AcO}), 19.8 (Me_{AcO}).

Synthesis of [{Pt(bisNHC-C4)}$_2${μ-(S-*p*-tol)}$_2$](PF$_6$)$_2$ ([2](PF$_6$)$_2$)

[**2**](PF$_6$)$_2$ was synthesised following the same procedure as that used for [**1**](PF$_6$)$_2$, except that [Pt(bisNHC-C4)(NCMe)$_2$](PF$_6$)$_2$ (323 mg, 0.22 mmol) was used in place of [Pt(bisNHC-C2)(NCMe)$_2$](PF$_6$)$_2$. Yield: 251 mg (84%). Single crystals suitable for X-ray crystallographic analysis were obtained in a similar manner to that used for [**1**](PF$_6$)$_2$. Anal. calcd for [**2**](PF$_6$)$_2$·0.5CH_2Cl_2·0.5tol ($C_{101.5}H_{119}F_{12}N_8O_{36.5}P_2Pt_2S_2$): C, 43.86; H, 4.32; N, 4.03. Found: C, 43.92; H, 4.61; N, 4.29. MS (ESI+, CH_3CN): *m*/*z* = 1216.59 (1216.31 calcd for [**2**]$^{2+}$ and [(**2**)/2]$^+$), 2577.56 (2577.57 calcd for [(**2**) + PF$_6$]$^+$). ^{1}H NMR (CD_3CN, 600 MHz, 298 K): δ 7.58 (Xy, 4H, m), 7.46 (tol, 4H, d, ^3J = 6.7 Hz), 7.38 (Xy, 4H, m), 7.14 (4-Im$_{tb}$, 2H, d, ^3J = 2.0 Hz), 7.08 (5-Im$_{tb}$, 2H, d, ^3J = 2.2 Hz), 7.05 (tol, 4H, d, ^3J = 7.5 Hz), 7.02 (5-Im$_c$, 2H, d, ^3J = 1.9 Hz), 6.89 (4-Im$_c$, 2H, d, ^3J = 2.0 Hz), 6.83 (CH_2-Im$_{tb}$, 2H, d, ^3J = 14.5 Hz), 6.67 (CH_2-Im$_c$, 2H, d, ^3J = 14.7 Hz), 6.58 (1-Glc$_c$, 2H, d, ^3J = 9.4 Hz), 6.49 (1-Glc$_{tb}$, 2H, s), 5.73 (2-Glc$_{tb}$, 2H, d, ^3J = 3.7 Hz), 5.54 (3-Glc$_c$, 2H, t, ^3J = 9.5 Hz), 5.46 (2-Glc$_c$, 2H, t, ^3J = 9.0 Hz), 5.40 (4-Glc$_c$, 2H, t, ^3J = 9.6 Hz), 5.33 (3-Glc$_{tb}$, 2H, d, ^3J = 3.2 Hz), 5.04 (CH_2-Im$_{tb}$, 2H, d, ^3J = 13.8 Hz), 5.03 (4-Glc$_{tb}$, 2H, d, ^3J = 9.4 Hz), 4.92 (CH_2-Im$_c$, 2H, d, ^3J = 14.9 Hz), 4.66 (6-Glc$_c$, 2H, dd, ^2J = 13.2 Hz, ^3J = 2.1 Hz), 4.59 (6-Glc$_c$, 2H, dd, ^2J = 13.2 Hz, ^3J = 1.6 Hz), 4.35 (5-Glc$_{tb}$, 2H, m), 4.31 (5-Glc$_c$, 2H, d, ^3J = 10.2 Hz), 4.08 (6-Glc$_{tb}$, 2H, dd, ^2J = 12.7 Hz, ^3J = 2.6 Hz), 4.03 (6-Glc$_{tb}$, 2H, dd, ^2J = 12.7 Hz, ^3J = 5.5 Hz), 2.55 (Me$_{tol}$, 6H, s), 2.32 (Me_{AcO}, 6H, s), 2.12 (Me_{AcO}, 6H, s), 2.11 (Me_{AcO}, 6H, s), 2.06 (Me_{AcO}, 6H, s), 1.94 (Me_{AcO}, 6H, s), 1.81 (Me_{AcO}, 6H, s), 1.75 (Me_{AcO}, 6H, s), 0.65 (Me_{AcO}, 6H, s). ^{13}C NMR (CD_3CN, 150 MHz, 298 K): δ 171.4 (CO_{AcO}), 171.3 (CO_{AcO}), 171.1 (CO_{AcO}), 170.7 (CO_{AcO}), 170.5 (CO_{AcO}), 170.4 (CO_{AcO}), 169.43 (CO_{AcO}), 169.41 (CO_{AcO}), 155.3 (2-Im$_c$), 152.7 (2-Im$_{tb}$), 140.2 (tol), 135.6 (Xy), 134.9 (Xy), 134.4 (tol), 131.8 (Xy), 130.8 (Xy), 130.2 (3-tol), 126.1 (4-tol), 123.8 (5-Im$_c$), 122.6 (4-Im$_{tb}$), 121.4 (5-Im$_{tb}$), 120.6 (4-Im$_c$), 87.6 (1-Glc$_c$), 87 (1-Glc$_{tb}$), 76.4 (5-Glc$_c$), 73.5 (3-Glc$_c$), 72.4 (5-Glc$_{tb}$), 71.8 (2-Glc$_{tb}$), 70.1 (2-Glc$_c$), 69.1 (3-Glc$_{tb}$), 68.8 (4-Glc$_c$), 68.5 (4-Glc$_{tb}$), 63.9 (6-Glc$_{tb}$), 61.5 (6-Glc$_c$), 53.2 (CH_2-Im$_{tb}$), 52.6 (CH_2-Im$_c$), 21.8 (Me$_{tol}$), 21.1 (Me_{AcO}), 21.1 (Me_{AcO}), 21 (Me_{AcO}), 20.9 (Me_{AcO}), 20.84 (Me_{AcO}), 20.78 (Me_{AcO}), 18.9 (Me_{AcO}).

Reactions of diplatinum complexes [1](PF$_6$)$_2$ or [2](PF$_6$)$_2$ with a Grignard reagent

A solution of 2-fluorophenylmagnesium bromide (4.8 μmol) was added to a solution of [**1**](PF$_6$)$_2$ (5.1 mg, 2.0 μmol) or [**2**](PF$_6$)$_2$ (5.4 mg, 2.0 μmol) in the presence of CuI (1.0 mmol L^{-1} solution in THF, 0.100 mL, 0.1 μmol) in THF (0.5 mL), and the mixture was stirred under a N_2 atmosphere for 3 h. A saturated solution of NH_4Cl (1 mL) was added, and the products were extracted with CH_2Cl_2 (1 mL). The solvent of the separated organic layer was removed under reduced pressure. The residue was dissolved in $CDCl_3$ for NMR measurements.

X-Ray crystallographic analyses of [1](PF$_6$)$_2$ and [2](PF$_6$)$_2$

Single crystals of [**1**](PF$_6$)$_2$ and [**2**](PF$_6$)$_2$ were mounted on loops using Paratone oil. X-ray diffraction data were collected on a Rigaku VariMax Saturn724 diffractometer using the rotation method with 0.5° frame widths, controlled by CrystalClear[16] software. The data were integrated, scaled, sorted and averaged using CrysAlisPro (version 1.171.44.85).[17]

Absorption corrections were applied using the multi-scan method. The structures were solved by direct methods using SHELXS97[18] and refined by full-matrix least-squares on F^2 using SHELXL (version 2018/3).[19] All hydrogen atoms were placed in calculated positions and refined as a riding model. Crystallographic data are summarised in Tables S1 and S2 in the SI. The structures exhibit positional disorder in AcO groups and solvent molecules. Owing to difficulties in achieving satisfactory refinement of the disordered solvent regions, a solvent mask was applied using the PLATON/SQUEEZE procedure.[20]

DFT calculations of diplatinum complexes

DFT calculations were performed on $[\mathbf{1}]^{2+}$ and $[\mathbf{2}]^{2+}$, as well as their selected C_2-symmetric isomers, using Gaussian 16.[21] Geometry optimisations were carried out at the B3LYP/LanL2DZ level of theory. Initial geometries for $[\mathbf{1}]^{2+}$ and $[\mathbf{2}]^{2+}$ were taken from the corresponding crystallographic structures, while those for the isomers were generated by appropriate structural modification. Vibrational frequency calculations were performed for all optimised structures, and no imaginary frequencies were observed, confirming that the structures correspond to true minima on the potential energy surface. The atomic coordinates of the optimised structures are listed in Tables S3–S10 in the SI.

Author contributions

Shuhei Nomura: syntheses, performing reactions, characterisation and crystal structures; Itsuki Kobayashi: syntheses and characterisation; Matsumi Doe: NMR spectroscopy; Rika Tanaka: crystal structures; Tamaki Nagasawa: elemental analyses; Takanori Nishioka: supervision, conceptualisation, characterisation, crystal structures, funding and writing.

Conflicts of interest

There are no conflicts to declare.

Data availability

The data supporting this article have been included as part of the supplementary information (SI). Supplementary information is available: experimental details, NMR and mass spectra, X-ray crystallographic data and DFT calculations. See DOI: https://doi.org/10.1039/d6dt00111d.

CCDC 2518861 and 2518862 contain the supplementary crystallographic data for this paper.[22a,b]

Acknowledgements

This work was supported by JSPS KAKENHI (Grant Number N22K05146).

References

1 (*a*) R. M. Thomas, A. Fedorov, B. K. Keitz and R. H. Grubbs, *Organometallics*, 2011, **30**, 6713; (*b*) V. Paradiso, V. Bertolasi, C. Costabilea and F. Grisi, *Dalton Trans.*, 2016, **45**, 561.

2 (*a*) T. A. P. Paulose, J. A. Olson, J. W. Quail and S. R. Foley, *J. Organomet. Chem.*, 2008, **693**, 3405; (*b*) D. Munz, C. Allolio, D. Meyer, M. Micksch, L. Roessner and T. Strassner, *J. Organomet. Chem.*, 2015, **794**, 330; (*c*) J. Berding, M. Lutz, A. L. Spek and E. Bouwman, *Organometallics*, 2009, **28**, 1845.

3 (*a*) A. L. Ostericher, K. M. Waldie and C. P. Kubiak, *ACS Catal.*, 2018, **8**, 9596; (*b*) A. L. Ostericher, T. M. Porter, M. H. Reineke and C. P. Kubiak, *Dalton Trans.*, 2019, **48**, 15841.

4 (*a*) L. C. Silva, P. T. Gomes, L. F. Veiros, S. I. Pascu, M. T. Duarte, S. Namorado, J. R. Ascenso and A. R. Dias, *Organometallics*, 2006, **25**, 4391; (*b*) G. S. Nichol, J. Rajaseelan, L. J. Anna and E. Rajaseelan, *Eur. J. Inorg. Chem.*, 2009, 4320; (*c*) A. M. Ortiz, P. Gómez-Sal, J. C. Flores and E. de Jesús, *Organometallics*, 2014, **33**, 600; (*d*) M. M. D. Roy, P. A. Lummis, M. J. Ferguson, R. McDonald and E. Rivard, *Chem. – Eur. J.*, 2017, **23**, 11249; (*e*) R. Fraser, C. G. C. E. van Sittert, P. H. van Rooyen and M. Landman, *J. Organomet. Chem.*, 2017, **835**, 60; (*f*) J. Oberkofler, B. Aikman, R. Bonsignore, A. Pöthig, J. Platts, A. Casini and F. E. Kühn, *Eur. J. Inorg. Chem.*, 2020, 1040.

5 (*a*) I. C. Stewart, C. J. Douglas and R. H. Grubbs, *Org. Lett.*, 2008, **10**, 441; (*b*) A. Perfetto, V. Bertolasi, C. Costabile, V. Paradiso, T. Caruso, P. Longoa and F. Grisi, *RSC Adv.*, 2016, **6**, 95793; (*c*) A. M. Ortiz, A. Sánchez-Méndez, E. de Jesús, J. C. Flores, P. Gómez-Sal and F. Mendicuti, *Inorg. Chem.*, 2016, **55**, 1304; (*d*) G. A. Andrade, J. L. DiMeglio, E. T. Guardino, G. P. A. Yap and J. Rosenthal, *Polyhedron*, 2017, **135**, 134; (*e*) L. Le, J. Liu, T. He, D. Kim, E. J. Lindley, T. N. Cervarich, J. C. Malek, J. Pham, M. R. Buck and A. R. Chianese, *Organometallics*, 2018, **37**, 3286; (*f*) T. Mandal, S. Yadav and J. Choudhury, *J. Organomet. Chem.*, 2021, **953**, 122047; R. Kadyrov, *J. Catal.*, 2023, **426**, 173; (*g*) N. Şahin, *Inorg. Chim. Acta*, 2025, **574**, 122355.

6 (*a*) D. Saito, T. Ogawa, M. Yoshida, J. Takayama, S. Hiura, A. Murayama, A. Kobayashi and M. Kato, *Angew. Chem., Int. Ed.*, 2020, **59**, 18723; (*b*) H. Uesugi, T. Tsukuda, K. Takaoa and T. Tsubomura, *Dalton Trans.*, 2013, **42**, 7396; (*c*) J.-L. Liao, Y. Chi, J.-Y. Wang, Z.-N. Chen, Z.-H. Tsai, W.-Y. Hung, M.-R. Tseng and G.-H. Lee, *Inorg. Chem.*, 2016, **55**, 6394.

7 (*a*) R. E. Douthwaite, D. Haüssinger, M. L. H. Green, P. J. Silcock, P. T. Gomes, A. M. Martins and A. A. Danopoulos, *Organometallics*, 1999, **18**, 4584; (*b*) N. Muthukumaran, S. Arruri, M. Vaddamanu, R. Karupnaswamy, M. Mannarsamy, M. Adinarayana and P. Ganesan, *Polyhedron*, 2019, **158**, 125; (*c*) M. Nirmala, G. Saranya, P. Viswanathamurthi, R. Bertani, P. Sgarbossa and J. G. Malecki, *J. Organomet. Chem.*, 2017, **831**, 1; (*d*) J. Guo, L. Lv, X. Wang, C. Cao, G. Pang and Y. Shi, *Inorg. Chem. Commun.*, 2013, **31**, 74; (*e*) H. M. Lee, C. Y. Lu,

C. Y. Chen, W. L. Chen, H. C. Lin, P. L. Chiu and P. Y. Cheng, *Tetrahedron*, 2004, **60**, 5807; (*f*) Q. Teng and H. V. Huynh, *Inorg. Chem.*, 2014, **53**, 10964.

8 (*a*) S. Ahrens, A. Zeller, M. Taige and T. Strassner, *Organometallics*, 2006, **25**, 5409; (*b*) M. Nonnenmacher, D. Kunz, F. Rominger and T. Oeser, *J. Organomet. Chem.*, 2007, **692**, 2554; (*c*) A. Biffis, L. Gazzola, P. Gobbo, G. Buscemi, C. Tubaro and M. Basato, *Eur. J. Org. Chem.*, 2009, 3189; (*d*) T.-H. Hsiao, T.-L. Wua, S. Chatterjee, C.-Y. Chiu, H. M. Lee, L. Bettucci, C. Bianchini and W. Oberhauser, *J. Organomet. Chem.*, 2009, **694**, 4014; (*e*) H. V. Huynh and R. Jothibasu, *J. Organomet. Chem.*, 2011, **696**, 3369; (*f*) X.-F. Hou, Y.-N. Wang and I. Göttker-Schnetmann, *Organometallics*, 2011, **30**, 6053; (*g*) Y. Maeda, H. Hashimoto, I. Kinoshita and T. Nishioka, *Inorg. Chem.*, 2014, **53**, 661; (*h*) W. Mansour, M. Fettouhi and B. E. Ali, *Appl. Organomet. Chem.*, 2020, **34**, 5636; (*i*) J. De Tovar, F. Rataboul and L. Djakovitch, *ChemCatChem*, 2020, **12**, 5797; (*j*) Y. Maeda, H. Hashimoto, I. Kinoshita and T. Nishioka, *Inorg. Chem.*, 2015, **54**, 448; (*k*) N. Yabune, H. Nakajima and T. Nishioka, *Dalton Trans.*, 2020, **49**, 7680; (*l*) N. Yabune, H. Nakajima and T. Nishioka, *Dalton Trans.*, 2021, **50**, 12079; (*m*) P. Pinter, A. Biffis, C. Tubaro, M. Tenne, M. Kalinerb and T. Strassner, *Dalton Trans.*, 2015, **44**, 9391.

9 (*a*) Y. Imanaka, H. Hashimoto, I. Kinoshita and T. Nishioka, *Chem. Lett.*, 2014, **43**, 687; (*b*) Y. Imanaka, H. Hashimoto and T. Nishioka, *Bull. Chem. Soc. Jpn.*, 2015, **88**, 1135; (*c*) Y. Imanaka, N. Shiomoto, M. Tamaki, Y. Maeda, H. Nakajima and T. Nishioka, *Bull. Chem. Soc. Jpn.*, 2017, **90**, 59; (*d*) Y. Imanaka, K. Nakao, Y. Maeda and T. Nishioka, *Bull. Chem. Soc. Jpn.*, 2017, **90**, 1050.

10 T. Shibata, H. Hashimoto, I. Kinoshita, S. Yano and T. Nishioka, *Dalton Trans.*, 2011, **40**, 4826.

11 (*a*) X. Moreau, J. M. Campagne, G. Meyer and A. Jutand, *Eur. J. Org. Chem.*, 2005, 3749; (*b*) J. F. Hartwig, *Nature*, 2008, **455**, 314; (*c*) Y. Zhang, K. C. Ngeow and J. Y. Ying, *Org. Lett.*, 2007, **9**, 3495; (*d*) M. A. Fernandez-Rodriguez, Q. Shen and J. F. Hartwig, *J. Am. Chem. Soc.*, 2006, **128**, 2180; (*e*) F. Abedinifar, S. Bahadorikhalili, B. Larijani, M. Mahdavi and F. Verpoort, *Appl. Organomet. Chem.*, 2022, **36**, 6482.

12 (*a*) P. A. Mane, S. Dey, A. K. Pathak, M. Kumar and N. Bhuvanesh, *Inorg. Chem.*, 2019, **58**, 2965; (*b*) S. Bernès, L. Villanueva and H. Torrens, *J. Chem. Crystallogr.*, 2008, **38**, 123; (*c*) G. Rivera, S. Bernès, C. R. de Barbarin and H. Torrens, *Inorg. Chem.*, 2001, **40**, 5575; (*d*) Y. A. Kovelenov, A. J. Blake, M. W. George, P. Matousek, M. Ya. Mel'nikov, A. W. Parker, X.-Z. Sun, M. Towrie and J. A. Weinstein, *Dalton Trans.*, 2005, 2092; (*e*) L. Villanueva, M. Arroyo, S. Bernès and H. Torrens, *Chem. Commun.*, 2004, 1942; (*f*) J. J. Garcia, A. Arevalo, V. Montiel, F. Del Rio, B. Quiroz, H. Adams and P. M. Maitlis, *Organometallics*, 1997, **16**, 3216; (*g*) C. Albrecht, S. Schwieger, C. Bruhn, C. Wagner, R. Kluge, H. Schmidt and D. Steinborn, *J. Am. Chem. Soc.*, 2007, **129**, 4551; (*h*) S. E. Castillo-Blum, M. Flores-Alamo, D. Franco-Bodek, G. Hernandez and H. Torrens, *Inorg. Chem. Commun.*, 2014, **45**, 44; (*i*) G. Rivera, S. Bernès and H. Torrens, *Polyhedron*, 2007, **26**, 4276; (*j*) S.-K. Lee, O. Jeannin, M. Fourmigué, W. Suh and D.-Y. Noh, *J. Organomet. Chem.*, 2012, **716**, 237; (*k*) N. Ghavale, A. Wadawale, S. Dey and V. K. Jain, *J. Organomet. Chem.*, 2010, **695**, 2296; (*l*) V. K. Jain, S. Kannan, R. J. Butcher and J. P. Jasinski, *J. Organomet. Chem.*, 1994, **468**, 285.

13 (*a*) G. Altenhoff, R. Goddard, C. W. Lehmann and F. Glorius, *J. Am. Chem. Soc.*, 2004, **126**, 15195; (*b*) S. Würtz, C. Lohre, R. Fröhlich, K. Bergander and F. Glorius, *J. Am. Chem. Soc.*, 2009, **131**, 8344; (*c*) V. Lavallo, Y. Canac, C. Präsang, B. Donnadieu and G. Bertrand, *Angew. Chem., Int. Ed.*, 2005, **44**, 5705; (*d*) S. Würtz and F. Glorius, *Acc. Chem. Res.*, 2008, **41**, 1523–1533.

14 K. Halikowska-Tarasek, W. Ochędzan-Siodłak, B. Dziuk, R. Szostak, M. Szostak and E. Bisz, *Inorg. Chem.*, 2025, **64**, 7851.

15 T. Matsuzawa, K. Uchida, S. Yoshida and T. Hosoya, *Org. Lett.*, 2017, **19**, 5521.

16 *CrystalClear*, Rigaku Corporation, 1999; *CrystalClear Software User's Guide*, Molecular Structure Corporation, 2000; J. W. Pflugrath, *Acta Crystallogr., Sect. D:Biol. Crystallogr.*, 1999, **55**, 1718–1725.

17 *CrysAlis PRO*, Rigaku Oxford Diffraction, Yarnton, England, 2023.

18 SHELXL97; G. M. Sheldrick, *Program for crystal structure refinement*, University of Göttingen, Göttingen, Germany, 1997.

19 G. M. Sheldrick, *Acta Crystallogr., Sect. A:Found. Crystallogr.*, 2008, **64**, 112–122.

20 A. L. Spek, *Acta Crystallogr., Sect. C:Struct. Chem.*, 2015, **71**, 9–18.

21 M. J. Frisch, G. W. Trucks, H. B. Schlegel, G. E. Scuseria, M. A. Robb, J. R. Cheeseman, G. Scalmani, V. Barone, G. A. Petersson, H. Nakatsuji, X. Li, M. Caricato, A. V. Marenich, J. Bloino, B. G. Janesko, R. Gomperts, B. Mennucci, H. P. Hratchian, J. V. Ortiz, A. F. Izmaylov, J. L. Sonnenberg, D. Williams-Young, F. Ding, F. Lipparini, F. Egidi, J. Goings, B. Peng, A. Petrone, T. Henderson, D. Ranasinghe, V. G. Zakrzewski, J. Gao, N. Rega, G. Zheng, W. Liang, M. Hada, M. Ehara, K. Toyota, R. Fukuda, J. Hasegawa, M. Ishida, T. Nakajima, Y. Honda, O. Kitao, H. Nakai, T. Vreven, K. Throssell, J. A. Montgomery Jr., J. E. Peralta, F. Ogliaro, M. J. Bearpark, J. J. Heyd, E. N. Brothers, K. N. Kudin, V. N. Staroverov, T. A. Keith, R. Kobayashi, J. Normand, K. Raghavachari, A. P. Rendell, J. C. Burant, S. S. Iyengar, J. Tomasi, M. Cossi, J. M. Millam, M. Klene, C. Adamo, R. Cammi, J. W. Ochterski, R. L. Martin, K. Morokuma, O. Farkas, J. B. Foresman and D. J. Fox, *Gaussian 16, Revision C.01*, Gaussian, Inc., Wallingford CT, 2016.

22 (*a*) CCDC 2518861: Experimental Crystal Structure Determination, 2026, DOI: 10.5517/ccdc.csd.cc2qk2lz; (*b*) CCDC 2518862: Experimental Crystal Structure Determination, 2026, DOI: 10.5517/ccdc.csd.cc2qk2m0.

